Energy Proceedings
2022
ISSN 2004-2965

Modeling of the Thermal Behaviors of Silicon/Graphite Composite Electrodes for Lithium-ion Batteries

Zirui Shao[1], Yang Jiang[1]*, Gregory Offer[1,2], Huizhi Wang[1,2]

1 Department of Mechanical Engineering, Imperial College London, United Kingdom
2 The Faraday Institution, Harwell Science and Innovation Campus, Didcot, United Kingdom

ABSTRACT

Silicon/graphite composite electrodes are promising because of their high capacities, and much research has been conducted to speed up the commercialization of lithium-ion batteries with silicon/graphite electrodes. However, most of the research focuses on electrochemical and mechanical behaviors of the composite electrodes, and thermal behavior analysis of silicon/graphite electrodes is scarce. It is necessary to study the thermal behavior because it hugely affects the performance and safe operation of lithium-ion batteries. This study for the first time develops an electrochemical-thermal model for silicon/graphite electrodes based on a multi-material framework, which can separate the electrochemical and thermal behaviors of each electrode material. Using the model, the thermal characteristics of silicon/graphite electrodes are investigated. The research reveals the relationship between heat, characteristics of active materials, and their content in the composite electrode. At the same C-rate, an electrode with a higher silicon content experiences a higher temperature rise. Thermal peaks representing the phase transition processes of graphite are observed during (de)lithiation, which can be potentially used to detect the aging of silicon-based batteries in service. We further analyze the contributions of different heat sources. The heat generation of graphite converges on the beginning stage of delithiation followed by huge heat generation from silicon. In contrast, the two active materials are lithiated simultaneously, and graphite plays a dominant role during its phase transition processes. For a composite electrode with a mass ratio of silicon to graphite of 0.2 at a moderate C rate (2C), ohmic heat generation is the major contributor to heat generation accounting for 41% of the total heat generation, followed by reversible (36.1%) and irreversible (22.9%) heat generation. This model paves the way for experimental work regarding the thermal characteristics of silicon/graphite composite electrodes and can be potentially used for the thermal analysis of large-format batteries with silicon/graphite electrodes in the electrical vehicle industry.

Keywords: Li-ion battery, silicon anode, thermo-electrochemical model

NONMENCLATURE

A	Cross-section area of electrode (m^2)
a_s	Specific surface area of active solid material particles (m^{-1})
c_e	Electrolyte concentration (mol m^{-3})
c_s	Lithium concentration (mol m^{-3})
C_p	Specific heat capacity (J kg^{-1} K^{-1})
C_{rate}	C-rate
D_e	Electrolyte diffusivity (m^2 s^{-1})
D_s	Diffusivity of lithium in solid phase (m^2 s^{-1})
E	Output voltage (V)
E^D	Solid-phase diffusion activation energy (J mol^{-1})
E^r	Reaction constant activation energy (J mol^{-1})
F	Faraday constant (C mol^{-1})
$f_\pm$	Mean molar activity coefficient of electrolyte
h	Convective heat transfer coefficient (J K^{-1})
i	Interfacial current density (A m^{-2})
i_0	Exchange current density (A m^{-2})
i_{app}	Applied current density (A m^{-2})
j	Volumetric current density (A m^{-3})
k	Rate constant ($m^{2.5}$ $mol^{-0.5}$ s^{-1})
l	Characteristic length of active solid material particles (m)
L	Thickness (μm)
mr	Mass fraction of silicon
Q	Volumetric heat generation (W m^{-3})
r	Particle radius (m)
R	Universal gas constant (J mol^{-1} K^{-1})
t	Time (s)
t_+^0	Transference number
T	Temperature (K)
U	Open circuit voltage (V)
x	Spatial variable (m)

This is a paper for the 14th International Conference on Applied Energy - ICAE2022, Aug. 8-11, 2022, Bochum, Germany.

Greek letters

α_a	Anodic transfer coefficients
α_c	Cathodic transfer coefficients
δ	Thickness of mesh
ϵ	Volume fraction
η	Overpotential (V)
θ	State of charge
k	Ionic conductivity (S m^{-1})
k_D	Diffusion conductivity (A m^{-1})
λ	Thermal conductivity (W m^{-1} K^{-1})
ρ	Density (kg m^{-3})
σ	Solid phase conductivity (S m^{-1})
ϕ_e	Electrolyte potential (V)
ϕ_s	Solid phase potential (V)

Subscripts and superscripts

amb	Ambient temperature
avg	Average
CE	Counter electrode
eff	Effective
Gr	Graphite
init	Initial
max	Maximum
min	Minimum
sep	Separator
surf	Surface
WE	Working electrode

1. INTRODUCTION

Climate change and urban sprawl appeal for a more sustainable mean of transportation. Under this circumstance, the concept of zero carbon transportation has been raised and promoted. On the one hand, it is important to construct more clean power plants by using hydropower, photovoltaic power, and wind etc. On the other hand, as one key element in future clean energy supply chain, energy storage device is one of the most important components in electric vehicle (EV) industry. After decades of research, batteries with different chemistries have been developed including lead acid battery, nickel metal and lithium-ion battery (LIB). However, as the energy storage device of EVs, LIB is more promising compared to other types because of high energy density, high power density and no memory effect. The energy densities of commercial LIBs with graphite (Gr) anode are around 150-180 Wh/kg. [1] The high energy density is expected to alleviate range anxiety and facilitate the popularization of EVs. This leads to widespread discussions whether to replace Gr anode with silicon/graphite (Si/Gr) composite anode in commercial products. The theoretical capacity of the Si electrode can reach around 4200 mAh/g for $Li_{4.4}Si$, compared to traditional Gr anode whose theoretical capacity is only approximately 372 mAh/g for LiC_6. [1] Compared to Gr, the operating potential and maximum Li concentration of Si is higher which alleviate Li plating when a battery is cycling at high C-rate [2], and Si is more abundant on the earth which makes it cost efficient. [1]

However, the practical application of Si anode is still challenged. The huge volume change of Si during cycling can lead to strong mechanical stress in electrodes. This causes pulverization of electrodes and significantly decreases the capacity of Si electrodes. [3] In addition, the breaking and reformation of solid electrolyte interphase (SEI) during cycling gives rise to rapid depletion of electrolyte and lithium ions (Li-ion). [4] The coulombic efficiency and capacity of LIBs decrease due to the decline of ionic conductivity of electrolyte. [1]

To solve the problems mentioned above, a couple of solutions have been proposed. Nano structured Si such as Si nanowires was reported as an effective approach to accommodate the large internal strain of Si during cycling, which can significantly reduce the pulverization of Si. [5] Furthermore, the experiments conducted by Liu et al. showed that Si particles with a diameter smaller than 150 nm do not crack or fracture during cycling. [6] The reason is that the nano scaled particles means swift relaxation of mechanical stress during lithiation and delithiation. Moreover, a smaller diameter of particle shortens the path for mass transport, and the larger surface to volume ratio enhances rate capability. [7] Another solution to alleviate issues associated with large volumetric of Si electrode is to incorporate Si with Gr medium. The Gr matrix stabilizes SEI and accommodates strain caused by swelling and shrinkage to avoid the break of SEI. [8] Besides mitigating electrode volume change, Gr offers high electronical conductivity, enhances the coulombic efficiency and capacity retention of electrodes. [8] These indicate Si/Gr composite electrodes are more promising for practical applications.

The thermal characteristics of LIBs with Gr anodes have been widely investigated through both experiments and models. However, the thermal behaviours of Si/Gr anodes have rarely been reported. The thermal behaviours of Si/Gr electrodes can be different from Gr electrodes in that the thermal and chemical properties of Si are different in terms of thermal conductivity, heat capacity and solid phase conductivity, etc. Moreover, the characteristics of lithiation and delithiation of Si and Gr are totally different because graphite is an intercalation material and Si is an alloying material. [3]

It is clear from the above that silicon/graphite electrodes are promising for next-generation high-energy-density LIBs, but their thermal behaviours remain unclear. Therefore, the overall aim of this project is to model and analyse the thermal characteristics of Si/Gr electrodes. The specific objectives are as follows:

- To develop an electrochemical-thermal model for Si/Gr electrodes able to differentiate the thermal characteristics and behaviours of each active material.
- To study the effect of Si content in composite electrode on the thermal characteristics of electrodes in terms of heat contribution of active materials

2. MODEL DEVELOPEMENT

2.1 Computational domain

The computational domain of the model is shown in Fig. 1. This research focuses on the thermal behaviours of Si/Gr electrodes, so a half cell model is constructed with a Si/Gr electrode as a working electrode (WE), and Li metal as a reference and counter electrode (CE). A separator soaked with electrolyte is seated between two electrodes. The transport limiting effect incurred by Li metal electrode is negligible because it has significantly higher rate constant than Gr and Si. [9] *x* represents the thickness direction of the half cell. *x*=0 is the boundary between the composite electrode and the current collector, $\hat{x}_1$ is the boundary between separator and the composite electrode, and $\hat{x}_2$ is the interface between the CE and separator.

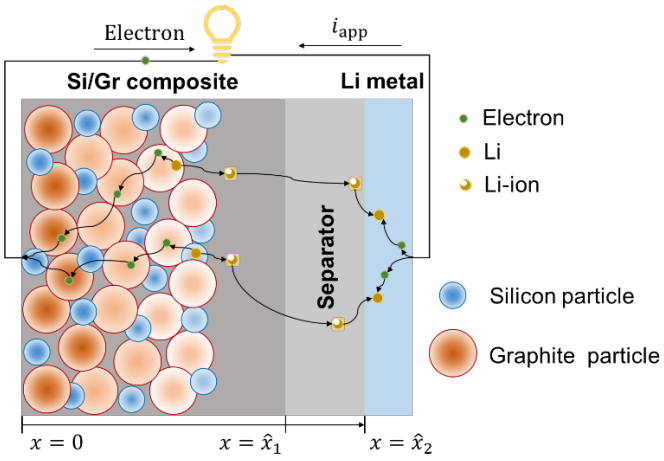

Fig. 1 The computational domain of model

2.2 Governing equations

The multi-material electrochemical model detailed in the previous paper by Jiang et al. [10] is used here with the governing equations and boundary conditions summarized in Table 1.

Table 1 Thermally coupled multi-material electrochemical model for Si/Gr composite electrodes. [10]

Description	Equation	Boundary conditions
	Composite electrode $\mathrm{k} \in \{\mathrm{Si}, \mathrm{Gr}\}$	
Mass conservation	$\frac{\partial(\epsilon_{\mathrm{s,k}} c_{\mathrm{s,k}})}{\partial t} = \frac{-a_{\mathrm{s,k}} i_{\mathrm{k}}}{F}$ $\frac{D_{\mathrm{s,k}}}{l_{\mathrm{k}}}\left(c_{\mathrm{s,k}}^{\mathrm{surf}} - c_{\mathrm{s,k}}\right) = \frac{-i_{\mathrm{k}}}{F} \quad l_{\mathrm{k}} = \frac{r_{\mathrm{k}}}{5} \quad a_{\mathrm{s,k}} = \frac{3\epsilon_{\mathrm{s,k}}}{r_{\mathrm{k}}}$	
Charge conservation	$\frac{\partial}{\partial x}\left(\sigma^{\mathrm{eff}} \frac{\partial \phi_{\mathrm{s}}}{\partial x}\right) - \mathrm{J} = 0$ $J = \sum_{\mathrm{k}} \left(i_{\mathrm{k}} a_{\mathrm{s,k}}\right)$	$\left.\frac{\partial \phi_{\mathrm{s}}}{\partial x}\right\|_{x=0} = -\frac{i_{\mathrm{app}}}{\sigma^{\mathrm{eff}}}$ $\left.\frac{\partial \phi_{\mathrm{s}}}{\partial x}\right\|_{x=\hat{x}_1} = 0$ $\phi_{\mathrm{s}}\|_{x=\hat{x}_2} = 0$
	Electrolyte	
Mass conservation	$\frac{\partial(\epsilon_{\mathrm{e}} c_{\mathrm{e}})}{\partial t} = \frac{\partial}{\partial x}\left(D_{\mathrm{e}}^{\mathrm{eff}} \frac{\partial c_{\mathrm{e}}}{\partial x}\right) + \frac{1-t_+^0}{F} J$	$\left.\frac{\partial c_{\mathrm{e}}}{\partial x}\right\|_{x=0} = 0$ $D_{\mathrm{e}}^{\mathrm{eff}} \left.\frac{\partial c_{\mathrm{e}}}{\partial x}\right\|_{x=\hat{x}_1^-} = D_{\mathrm{e}}^{\mathrm{eff}} \left.\frac{\partial c_{\mathrm{e}}}{\partial x}\right\|_{x=\hat{x}_1^+}$ $\left.\frac{\partial c_{\mathrm{e}}}{\partial x}\right\|_{x=\hat{x}_2} = -\frac{(1-t_+^0) i_{\mathrm{CE}}}{D_{\mathrm{e}}^{\mathrm{eff}} F}$

Charge conservation	$\frac{\partial}{\partial x}\left(\kappa^{\text{eff}}\frac{\partial \phi_{\text{e}}}{\partial x}\right)+\frac{\partial}{\partial x}\left(\kappa_{\text{D}}^{\text{eff}}\frac{\partial \ln c_{\text{e}}}{\partial x}\right)+J=0$ $\kappa_{\text{D}}^{\text{eff}}=\frac{2RT\kappa^{\text{eff}}}{F}(t_{+}^{0}-1)\left(1+\frac{\text{dln } f_{\pm}}{\text{dln } C_{\text{e}}}\right)$	$\left.\frac{\partial \phi_{\text{e}}}{\partial x}\right\|_{x=0}=0$ $\left.\kappa^{\text{eff}}\frac{\partial \phi_{\text{e}}}{\partial x}\right\|_{x=\hat{x}_1^-}=\left.\kappa^{\text{eff}}\frac{\partial \phi_{\text{e}}}{\partial x}\right\|_{x=\hat{x}_1^+}$ $\left.\frac{\partial \phi_{\text{e}}}{\partial x}\right\|_{x=\hat{x}_2}=-\frac{i_{\text{CE}}}{\kappa^{\text{eff}}}-\frac{\kappa_{\text{D}}^{\text{eff}}}{\kappa^{\text{eff}}}\frac{\partial \ln C_{\text{e}}}{\partial x}$
Heat Transfer $\quad n \in \{WE, CE\}$		
Energy conservation	$\rho_{\text{n}}C_{\text{p,n}}\frac{\partial T}{\partial t}=\frac{\partial}{\partial x}\left[\lambda_{\text{n}}\frac{\partial T}{\partial x}\right]+Q_{\text{gen,n}}$	$-\lambda_{\text{WE}}\left.\frac{\partial T}{\partial x}\right\|_{\text{x=0}}=h(T_{\text{amb}}-T)$ $-\lambda_{\text{sep}}\left.\frac{\partial T}{\partial x}\right\|_{x=\hat{x}_2}=h(T-T_{\text{amb}})$
Reaction kinetics $\quad k \in \{Si, Gr\}$		
Butler-Volmer	$i_{\text{k}}=i_{0,\text{k}}\left(\text{e}^{\frac{\alpha_{\text{a,k}}F\eta_{\text{k}}}{RT}}-\text{e}^{-\frac{\alpha_{\text{c,k}}F\eta_{\text{k}}}{RT}}\right)$ $i_{\text{CE}}=Fk_{\text{CE}}c_{\text{e}}^{0.5}\left(\text{e}^{\frac{\alpha_{\text{a,CE}}F(\phi_{\text{s}}-\phi_{\text{e}})}{RT}}-\text{e}^{-\frac{\alpha_{\text{c,CE}}F(\phi_{\text{s}}-\phi_{\text{e}})}{RT}}\right)$	
Exchange current	$i_{0,\text{k}}=k_{\text{k}}^{\text{eff}}F(c_{\text{e}})^{\alpha_{\text{a,k}}}\left(c_{\text{s,k}}^{\max}-c_{\text{s,k}}^{\text{surf}}\right)^{\alpha_{\text{a,k}}}\left(c_{\text{s,k}}^{\text{surf}}\right)^{\alpha_{\text{c,k}}}$	
Overpotential	$\eta_{\text{k}}=\phi_{\text{s}}-\phi_{\text{e}}-U_{\text{k}}$	

'+' and '-' represent the right- and left-hand side of a boundary respectively.

2.3 Additional equations

The equilibrium potential curves of it at reference temperature, $U_{\text{Gr,ref}}$ (V), is obtained by polynomial fitting on experiment data [11] , given by

$$\begin{aligned}U_{\text{Gr,ref}}=&-985.1(\theta_{\text{Gr}})^9+4503.8(\theta_{\text{Gr}})^8\\&-8624.5(\theta_{\text{Gr}})^7+8954.8(\theta_{\text{Gr}})^6\\&-5451.5(\theta_{\text{Gr}})^5+1965.6(\theta_{\text{Gr}})^4\\&-405.4(\theta_{\text{Gr}})^3+45(\theta_{\text{Gr}})^2-2.9\theta_{\text{Gr}}+0.3\end{aligned}\quad(1)$$

The OCV curves of Si during lithiation/delithiation was measured by Sethuraman et al. [12] Separate OCVs are used for lithiation and delithiation in the model because the voltage hysteresis is significant, shown in Fig. 2. The OCV of Si at a given state of charge (SOC) is obtained by interpolation.

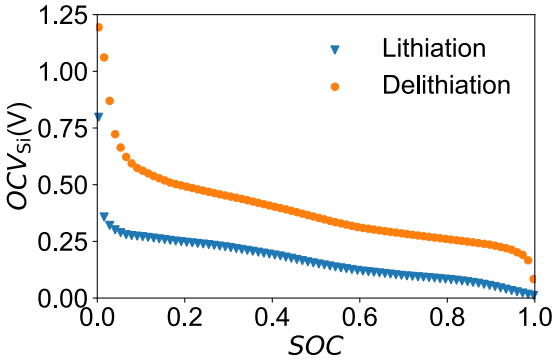

Fig. 2 OCVs of Si during lithiation/delithiation. [12]

The open circuit entropic variation of Gr, $\frac{\partial U_{\text{Gr}}}{\partial T}$ (V K^{-1}), is given by [13]

$$\left.\frac{\partial U_{\mathrm{Gr}}}{\partial T}\right|_{T_{\mathrm{ref}}} = 0.001 \frac{\begin{pmatrix} 0.005269056 \\ +3.2992657098\theta_{\mathrm{Gr}} \\ -91.7932579 8\theta_{\mathrm{Gr}}^2 \\ +1004.911008\theta_{\mathrm{Gr}}^3 \\ -5812.278127\theta_{\mathrm{Gr}}^4 \\ +19329.7549\theta_{\mathrm{Gr}}^5 \\ -37147.8947\theta_{\mathrm{Gr}}^6 \\ +38379.18127\theta_{\mathrm{Gr}}^7 \\ -16515.05308\theta_{\mathrm{Gr}}^8 \end{pmatrix}}{\begin{pmatrix} 1-48.09287227\theta_{\mathrm{Gr}} \\ +1017.234804\theta_{\mathrm{Gr}}^2 \\ -10481.80419\theta_{\mathrm{Gr}}^3 \\ +59431.3\theta_{\mathrm{Gr}}^4 \\ -195881.6488\theta_{\mathrm{Gr}}^5 \\ +374577.3152\theta_{\mathrm{Gr}}^6 \\ -385821.1607\theta_{\mathrm{Gr}}^7 \\ +165705.8597\theta_{\mathrm{Gr}}^8 \end{pmatrix}} \quad (2)$$

The entropy heat flow of Si anode was investigated by Housel and Arnot [14], [15] and it was demonstrated to be irreversible during lithiation and delithiation. The open circuit entropic variation of Si ($\frac{\partial U_{\mathrm{Si}}}{\partial T}$) as a function of SOC is obtained by linear regression, given by

$$\left.\frac{\partial U_{\mathrm{Si}}}{\partial T}\right|_{T_{\mathrm{ref}},\mathrm{Lithiation}} = \begin{matrix} 0.02068055\theta_{\mathrm{Si}}^5 - 0.06346280\theta_{\mathrm{Si}}^4 \\ +0.07164689\theta_{\mathrm{Si}}^3 - 0.03647035\theta_{\mathrm{Si}}^2 \\ +0.00812311\theta_{\mathrm{Si}} - 0.00030054 \end{matrix} \quad (3)$$

$$\left.\frac{\partial U_{\mathrm{Si}}}{\partial T}\right|_{\mathrm{T_{ref}},\mathrm{Delithiation}} = \begin{matrix} 0.01177207\theta_{\mathrm{Si}}^5 - 0.03358816\theta_{\mathrm{Si}}^4 \\ +0.03621296\theta_{\mathrm{Si}}^3 - 0.01869429\theta_{\mathrm{Si}}^2 \\ +0.00466615\theta_{\mathrm{Si}} - 0.00023652 \end{matrix} \quad (4)$$

The effective electric conductivity of composite electrode is calculated by the volume weighted conductivity of each material

$$\sigma^{\mathrm{eff}} = \sum_{\mathrm{k}} \sigma_{\mathrm{k}} \epsilon_{\mathrm{s,k}} \quad (5)$$

where σ_{k} (S m^{-1}) is the electric conductivity of active material k, and ϵ refers to its respective volume fraction.

2.4 Thermal dependent transport properties

The effective electrolyte diffusivity $D_{\mathrm{e}}^{\mathrm{eff}}$ (m^2 s^{-1}) is [13]

$$D_{\mathrm{e}}^{\mathrm{eff}} = \epsilon_{\mathrm{k}}^{\mathrm{brugg,k}} \times 10^{-4} \times 10^{-4.43 - \frac{54}{T-229-5\times10^{-3}c_{\mathrm{e}}} - 0.22\times10^{-3}c_{\mathrm{e}}} \quad (6)$$

where c_{e} (mol^{-1} m^{-3}) is electrolyte salt concentration, T (K) is temperature and brugg is Bruggeman factor.

The effective ionic conductivity κ_{eff} (S m^{-1}) is [13]

$$\kappa_{\mathrm{eff}} = \epsilon_{\mathrm{k}}^{\mathrm{brugg,k}} \times 10^{-4} \times c_{\mathrm{e}} \left(\begin{matrix} -10.5 + 0.668\cdot10^{-3}\cdot c_{\mathrm{e}} \\ +0.494\cdot10^{-6}c_{\mathrm{e}}^2 + \\ \left(0.074 - 1.78\times10^{-5}c_{\mathrm{e}}\right)T + \\ -8.86\times10^{-10}c_{\mathrm{e}}^2 \\ \left(-6.96\times10^{-5} + \right)T^2 \\ 2.8\times10^{-8}c_{\mathrm{e}} \end{matrix} \right)^2 \quad (7)$$

The thermal dependent equilibrium potentials of active materials are expressed as

$$U_{\mathrm{k}} = U_{\mathrm{k,\,ref}} + (T - T_{\mathrm{ref}}) \left.\frac{\partial U_{\mathrm{k}}}{\partial T}\right|_{T_{\mathrm{ref}}} \quad (8)$$

The effective reaction rate constant $k_{\mathrm{k}}^{\mathrm{eff}}$ (m$^{2.5}$ mol$^{-0.5}$ s^{-1}) is expressed as

$$k_{\mathrm{k}}^{\mathrm{eff}} = k_{\mathrm{k}} \mathrm{e}^{-\frac{E_{\mathrm{k}}^{\mathrm{r}}}{R}\left(\frac{1}{T}-\frac{1}{T_{\mathrm{ref}}}\right)} \quad (9)$$

where $E_{\mathrm{k}}^{\mathrm{r}}$ (J mol^{-1}) is reaction constant activation energy and R (J mol^{-1} K^{-1}) is universal gas constant.

The effective solid-phase diffusion coefficient $D_{\mathrm{eff,k}}^{\mathrm{s}}$ (m^2 s^{-1}) is

$$D_{\mathrm{eff,k}}^{\mathrm{s}} = D_{\mathrm{k}}^{\mathrm{s}} \mathrm{e}^{-\frac{E_{\mathrm{k}}^{\mathrm{D}}}{R}\left(\frac{1}{T}-\frac{1}{T_{\mathrm{ref}}}\right)} \quad (10)$$

where $E_{\mathrm{k}}^{\mathrm{D}}$ (J mol^{-1}) is the solid-phase diffusion activation energy.

2.5 Thermal properties and heat sources

The time derivative term of the composite electrode is expressed as the weighted average of the term for each active material

$$\rho_{\mathrm{WE}} C_{\mathrm{p,WE}} \epsilon_{\mathrm{s}} = \sum_{\mathrm{k}} \left(\rho_{\mathrm{k}} C_{\mathrm{p,k}} \epsilon_{\mathrm{k}}\right) \quad (11)$$

where ρ (kg m^{-3}) is density and C_{p} (J kg^{-1} K^{-1}) is specific heat capacity.

The thermal conductivity of composite anode can be expressed as [16]

$$\lambda_{\mathrm{eff}} = \lambda_{\mathrm{k}} (\epsilon_{\mathrm{k}})^{\mathrm{brugg,k}} \quad (12)$$

where λ_k (W m^{-1} K^{-1}) is the thermal conductivity for each material.

During the operation of LIBs, heat generation is inevitable. There are generally three types including reversible, irreversible and ohmic heat generation. The irreversible one is caused by the loss associated with kinetics limitation, while the ohmic heat generation is attributed to charge transport resistances. The reversible

heat generation is caused by the entropy change of the electrochemical intercalation/alloying reactions, which can be either positive or negative.

The irreversible heat generation, Q_{irr} (W m^{-3}), caused by the charge transfer reaction is given by

$$Q_{\mathrm{irr}} = J_{\mathrm{k}}\eta_{\mathrm{k}} \quad \mathrm{k} \in \{\mathrm{Gr}, \mathrm{Si}\} \tag{13}$$

where j is volumetric current density (A m^{-3}) and η (V) is overpotential.

The reversible heat sources due to the reaction entropic change (Q_{rev}) is expressed as

$$Q_{\mathrm{rev}} = J_{\mathrm{k}} T \left.\frac{\partial U_{\mathrm{k}}}{\partial T}\right|_{T_{\mathrm{ref}}} \tag{14}$$

The heat generation caused by the migration of electron ($Q_{\mathrm{ohm,ele}}$) is

$$Q_{\mathrm{ohm,ele}} = \sigma_{\mathrm{eff,k}} \left(\frac{\partial \phi_{\mathrm{s}}}{\partial x}\right)^2 \tag{15}$$

where ϕ_{s} is solid phase potential (V).

The heat generation caused by the Li ion transport is

$$Q_{\mathrm{ohm,ion}} = \kappa_{\mathrm{eff,k}} \left(\frac{\partial \phi_{\mathrm{e}}}{\partial x}\right)^2 + \frac{2\kappa_{\mathrm{eff,k}} RT}{F}(1 - t_+^0)\frac{\partial \ln c_{\mathrm{e}}}{\partial x}\frac{\partial \phi_{\mathrm{e}}}{\partial x} \tag{16}$$

where ϕ_{e} (V) is electrolyte potential, t_+^0 is transference number and F (C mol^{-1}) is Faraday's constant.

To normalize the heat generation obtained, the average volumetric heat generation per unit volume of active material, $Q_{\mathrm{k}}^{\mathrm{avg}}$, is introduced, which is given by

$$Q_{\mathrm{k}}^{\mathrm{avg}} = \frac{\sum Q\, \epsilon_{\mathrm{s,k}}\, A\, \delta}{\sum A\, \delta} \tag{17}$$

where A (μm^2) is the cross-section area of the electrode and δ (μm) is the thickness of each mesh.

2.6 Determination of other battery parameters

The SOC of the WE is determined by the volume averaged SOC of active materials

$$\theta_{\mathrm{WE}} = \frac{\sum_{\mathrm{k}} \left(c_{\mathrm{s,k}} \epsilon_{\mathrm{s,k}}\right)}{\sum_{\mathrm{k}} \left(c_{\mathrm{s,k}}^{\max} \epsilon_{\mathrm{s,k}}\right)} \tag{18}$$

Volume average method is also used to define the specific capacity of the WE

$$\mathrm{cap} = \frac{c_{\mathrm{s,WE}}\, F \sum_{\mathrm{k}} \epsilon_{\mathrm{s,k}}}{3600 \sum_{\mathrm{k}} \left(\epsilon_{\mathrm{s,k}} \rho_{\mathrm{k}}\right)} \tag{19}$$

The current density i_{app} (A m-2) applied to the battery can be estimated as

$$i_{\mathrm{app}} = \frac{L_{\mathrm{WE}} \sum_{\mathrm{k}} \left(c_{\mathrm{s,k}}^{\max} \epsilon_{\mathrm{s,k}}\right) F C_{\mathrm{rate}}}{3600} \tag{20}$$

where L_{WE} (μm) is the thickness of the WE, C_{rate} is the C-rate for charging or discharging, $c_{\mathrm{s,k}}^{\max}$ is the maximum Li concentration of active materials.

Mass ratio of Si over Gr ($r_{\mathrm{Si/Gr}}$) of a composite electrode is

$$r_{\mathrm{Si/Gr}} = \frac{\rho_{\mathrm{Si}} \epsilon_{\mathrm{s,Si}}}{\rho_{\mathrm{Gr}} \epsilon_{\mathrm{s,Gr}}} \tag{21}$$

2.7 Numerical procedures and model parameters

The model consists of differential equations for (k + 4) unknown field variables: $c_{\mathrm{s,k}}$, c_{e}, ϕ_{s}, ϕ_{e} and T. A finite volume method was used to discretize these differential equations, and the computation was repeated until convergence was achieved for all the field variables. The parameter values used for base case simulations are summarized in Table 2.

Table 2 Model parameters used in simulations

Symbol	Value	Unit	Ref.
$brugg_{\mathrm{Gr}}$	1.5		[10]
$brugg_{\mathrm{Si}}$	1.5		[10]
$c_{\mathrm{s,Gr}}^{\mathrm{init}}$	1854 for lithiation; 28405 for delithiation	$\mathrm{mol/m^3}$	[10]
$c_{\mathrm{s,Si}}^{\mathrm{init}}$	13025 for lithiation; 310090 for delithiation	$\mathrm{mol/m^3}$	[10]
$c_{\mathrm{s,Gr}}^{\max}$	30555	$\mathrm{mol/m^3}$	[13]
$c_{\mathrm{s,Si}}^{\max}$	311000	$\mathrm{mol/m^3}$	[10]
$c_{\mathrm{e}}^{\mathrm{init}}$	1000	$\mathrm{mol/m^3}$	[13]
ρ_{Gr}	2267	$\mathrm{kg/m^3}$	[13]
ρ_{Si}	2329	$\mathrm{kg/m^3}$	[10]
λ_{Gr}	1.7	$\mathrm{W/mK}$	[13]
λ_{Si}	2	$\mathrm{W/mK}$	[17]
$C_{\mathrm{p,Gr}}$	700	$\mathrm{kJ/kg}$	[13]
$C_{\mathrm{p,Si}}$	843	$\mathrm{kJ/kg}$	[18]
$D_{\mathrm{s,Gr}}$	3.9×10^{-14}	$\mathrm{m^2/s}$	[13]
$D_{\mathrm{s,Si}}$	3.0×10^{-16}	$\mathrm{m^2/s}$	[13]
D_e	7.5×10^{-10}	$\mathrm{m^2/s}$	[13]
$E_{\mathrm{Gr}}^{\mathrm{D}}$	5000	$\mathrm{J/mol}$	[13]
$E_{\mathrm{Si}}^{\mathrm{D}}$	41431	$\mathrm{J/mol}$	[19]
$E_{\mathrm{Gr}}^{\mathrm{r}}$	3600	$\mathrm{J/mol}$	[13]
$E_{\mathrm{Si}}^{\mathrm{r}}$	3600	$\mathrm{J/mol}$	
ϵ_{s}	0.4824		[13]
ϵ_{e}	0.41 in the WE; 0.724 in the separator		[13]
F	96485	$\mathrm{C/mol}$	

h	1.0	W/m K	[10]
k_{Gr}	5.031×10^{-11}	$\mathrm{m}^{2.5}/\mathrm{mol}^{0.5}\mathrm{s}$	[13]
k_{Si}	6×10^{-11}	$\mathrm{m}^{2.5}/\mathrm{mol}^{0.5}\mathrm{s}$	[10]
k_{CE}	1×10^{-4}	$\mathrm{m}^{2.5}/\mathrm{mol}^{0.5}\mathrm{s}$	[10]
α_{a}	0.5		
α_{c}	0.5		
R	8.314472	J/mol K	
r_{Gr}	2	μm	[10]
r_{Si}	0.3	μm	[10]
σ_{Gr}	100	S/m	[13]
σ_{Si}	33	S/m	[10]
t_+^0	0.364		[13]
A	300	$\mu\mathrm{m}^2$	[10]
L_{sep}	22	μm	[10]
L_{WE}	35	μm	[10]
δ	1	μm	[10]
T_{ref}	298.15	K	

3. RESULTS AND DISCUSSION

3.1 Temperature variation of composite electrode

Fig. 3(a) shows the temperature change of electrodes with different silicon fractions during delithiation process. For delithiation, temperature variations of composite electrodes with different Si content show a similar trend, increasing first followed by a drop, and concave profiles are observed during latter stage of the reaction, which present the same shape of that for pure Si. This implies that Si dominates the lower end of SOC during delithiation process for all these electrodes, supported by our previous study. [10] The temperature rises more significantly for composite electrodes with higher Si fractions. The reason is that the composite electrode with a higher Si fraction can provide more capacity, which leads to a higher current density at the same C-rate. As a result, more heat production and higher temperature increment will be seen in the composite electrode. Besides, as Si content increases, the thermal peaks shift to the left-hand side in Fig. 3(a), namely the higher end of SOC during delithiation. This is mainly because that a higher *mr* means a lower fraction of Gr, and hence its phase transition processes during delithiation will last for a shorter time.

In contrast, the temperature evolution with time during lithiation is different, displayed by Fig. 3(b). An initial temperature increase of the composite electrodes is seen due to the positive heat sources, and a first thermal peak is seen in Fig. 3(b). Three subsequent thermal peaks can be found for composite electrodes, which are caused by the competition of reaction rate of the two active materials. These thermal peaks increase in magnitude and shift to the right as the Si content increases. This is because the lithiation rate of Gr slows down with higher Si additives.

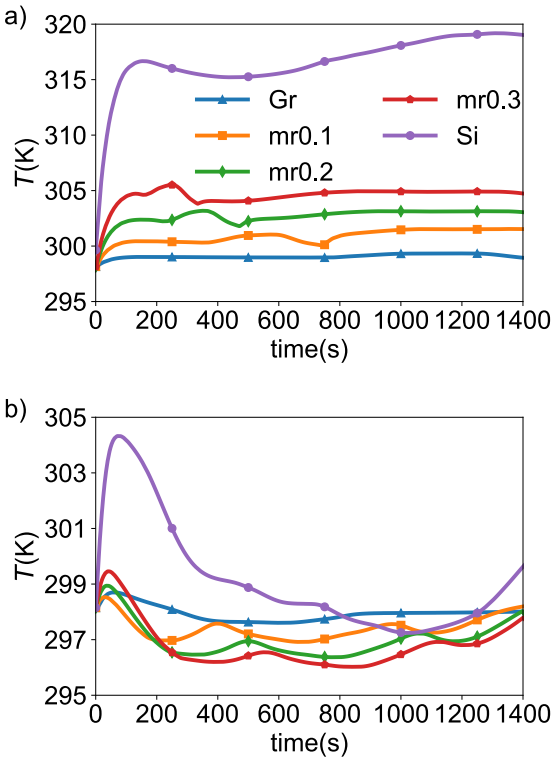

Fig. 3 Temperature variation of electrodes with different Si content during a) delithiation b) lithiation at a galvanostatic 2C condition, and h = 1W/(m K).

The composite electrodes are observed to experience more significant heat sink phenomenon compared to both pure Gr and Si electrodes (seen Fig. 3(b)), which is a compounded effect of two factors. The first factor is the maximum temperature reached by the first thermal peak, and the second factor is the total heat rejection during the reaction. The former is determined by the reversible heat generation of Si at high SOC which increases with the increased Si content, while the latter is determined by the total reversible heat rejection of Si and Gr at lower SOC.

Comparing Fig. 3(a) and (b), it is marked that the thermal behaviors during lithiation and delithiation are irreversible. This irreversibility derives from the asymmetric reaction kinetic behaviors of composite electrodes. [10] Another cause is the asymmetric entropic change of Si during lithiation and delithiation.

3.2 Analysis of contribution of different heat sources

The heat generation of two active materials during delithiation of an electrode with *mr* = 0.2 at a 2C condition is shown in Fig. 4(a). The heat generation of Gr

is found to dominate at the beginning of delithiation, which is in consistence with the research of Yao et al. who concluded that the delithiation of Gr is preferential at the initial stage of reaction when the electrode voltage (*E*) is lower than 0.23V. The reaction rate of Gr decreases between S2 and S3 when the electrode potential surpasses approximately 0.2V, which is close to the threshold observed in the research of Yao. [20]

The thermal behaviors of composite electrode are mostly affected by Gr over the initial stage of delithiation, where three thermal peaks can be observed in the temperature variation curve. The first two pronounced thermal peaks at S1 and S2 result from the large irreversible and reversible heat generation within these stages shown in Fig. 4(a). These high irreversible and reversible heat generations of Gr are determined by its high reaction rate, and they reach local maxima during the phase-transition processes of Gr (i.e. S1 and S2). The temperature declines after reaching the second thermal peak, where the boundary heat dissipation starts to surpass the heat production in the composite electrode. Then, the temperature decreases to a local minimum at S3. The reason is that Gr shows a sharp decrease in heat generation at S3 (seen in Fig. 4(a)), and the temperature climbs again to the third peak after the heat generation of Si starts to take place of Gr.

Before the end of S3, the heat generation of Si is only significant at the capacity intervals between phase transitions of Gr, when Si becomes more electrochemically active. The heat contribution of Gr decreases to zero after S3 when it is fully delithiated, and Si plays a major role in the thermal behaviors at the remaining part of the delithiation process shown in Fig. 4(a). The reversible heat generation of Si increases greatly and becomes a major contributor to the heat generation, while the irreversible heat generation of Si maintains insignificant throughout the reaction because the overpotential of Si electrode is relatively small during the reaction.

The temperature evolution with time during lithiation shows a different trend, displayed by Fig. 4(b). An initial temperature increase of the composite electrode is seen due to the reversible heat generation of Si. A huge drop in temperature is observed after the first thermal peak. Except for the boundary heat dissipation, the reversible heat of Si and Gr turns to be negative (seen in Fig. 4(b)) and outweighs the ohmic and irreversible heat, resulting in a heat sink phenomenon. Three heat rejection peaks can be found in the temperature curve for composite electrodes during lithiation, which could be attributed to the higher reaction rate of Si at these stages. The temperature profile is very similar to the heat contribution of Si (seen in Fig. 4(b)), while the effect of heat generation of Gr on temperature variation is not significant. This is because the reversible and irreversible heat of Gr are similar in magnitude and opposite in sign, so they are nearly cancelling out. The heat generation and rejection peaks of Gr are observed at S1, S2 and S3 (seen Fig. 4(b)) where Gr has high reaction rate. It is noted that the magnitude of peaks for the irreversible heat generation of Gr increases with time. This is caused by the increasing reaction rate of Gr when the electrode potential decreases.

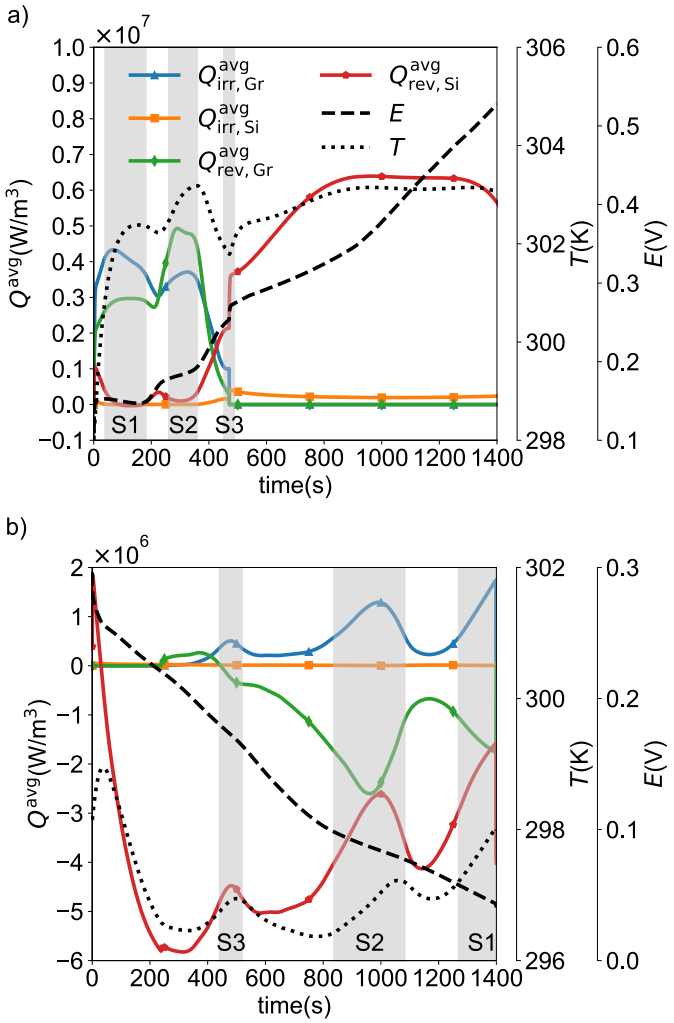

Fig. 4 Temperature variation and heat contribution attributed to active materials during a) delithiation b) lithiation for an electrode with mr = 0.2 at a galvanostatic 2C delithiation condition, and h = 1W/m K. Label S1 to S3 indicate the three phase transition processes of Gr.

The percentage of heat sources during delithiation of the electrode with mr= 0.1 at 2C is shown in Fig. 5. The ohmic heat accounts for the largest percentage of heat generation (41%), while the irreversible heat generation (22.9%) is the least significant ingredient. The

composite electrode is the major heat source that makes up 81.5% of total heat generation, compared to the separator. The heat generation for Gr (52.5%) accounts for a larger percentage of heat generation, compared to 6.5% of Si because the content of Gr is much higher than silicon in this case.

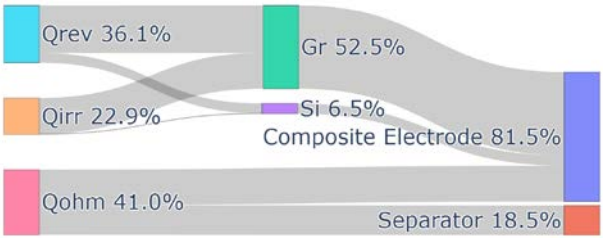

Fig. 5 Sankey chart for percentage contribution of heat sources when mr = 0.1 electrodes at a galvanostatic 2C delithiation condition.

4. CONCLUSIONS

In this study, a thermally coupled electrochemical model for Si/Gr composite electrodes is developed based on a multi-material model framework. This model is capable of separating different heat contributions of each active material by adopting their respective thermal properties and reaction rates. The temperature variation and different heat sources are analyzed for electrodes with different silicon fractions. Results show that observable thermal peaks can be identified during both lithiation and delithiation processes, corresponding to the phase transition processes of graphite. The thermal behaviors of composite electrodes are quite different between lithiation and delithiation processes, which can be attributed to the asymmetric entropic change and reaction kinetics of silicon. The thermal behavior of composite electrode is highly contingent on Si content, a transition from Gr to Si dominate electrode is witnessed in terms of temperature curve drift. The model is also used to analyze the contributions of different heat sources in different cell components and from different electrode materials. This thermal model for Si/Gr composite electrodes can be expanded to include thermally coupled degradation mechanisms in the future.

ACKNOWLEDGEMENT

This work was supported by the Faraday Institution (EP/S003053/1, FIRG003; FIRG038). For the purpose of open access, the authors have applied a 'creative commons attribution (CC BY) licence (where permitted by UKRI 'open government licence' or 'creative commons attribution no-derivatives (CC-BY-ND) licence' may be stated instead) to any author accepted manuscript version arising.

REFERENCE

[1] Li P, Zhao G, Zheng X, Xu X, Yao C, Sun W, Dou SX, Recent progress on silicon-based anode materials for practical lithium-ion battery applications, Energy Storage Mater. 2018;15:422–46

[2] Sturm J, Rheinfeld A, Zilberman I, Spingler FB, Kosch S, Frie F, Jossen A, Modeling and simulation of inhomogeneities in a 18650 nickel-rich, silicon-graphite lithium-ion cell during fast charging, J. Power Sources 2019;412:204–23

[3] Zhang WJ, A review of the electrochemical performance of alloy anodes for lithium-ion batteries, J. Power Sources 2011;196:13–24

[4] Casimir A, Zhang H, Ogoke O, Amine JC, Lu J, Wu G, Silicon-based anodes for lithium-ion batteries: Effectiveness of materials synthesis and electrode preparation, Nano Energy 2016;27:359–76

[5] Liu XH, Zheng H, Zhong L, Huang S, Karki K, Zhang LQ, Liu Y, Kushima A, Liang WT, Wang JW, Cho JH, Epstein E, Dayeh SA, Picraux ST, Zhu T, Li J, Sullivan JP, Cumings J, Wang C, Mao SX, Ye ZZ, Zhang S, Huang JY, Anisotropic swelling and fracture of silicon nanowires during lithiation, Nano Lett. 2011;11:3312–18

[6] Liu XH, Zhong L, Huang S, Mao SX, Zhu T, Huang JY, Size-dependent fracture of silicon nanoparticles during lithiation, ACS Nano 2012;6:1522–31

[7] Shen X, Tian Z, Fan R, Shao L, Zhang D, Cao G, Kou L, Bai Y, Research progress on silicon/carbon composite anode materials for lithium-ion battery, J. Energy Chem. 2018;27:1067–90

[8] Luo F, Liu B, Zheng J, Chu G, Zhong K, Li H, Huang X, Chen L, Review—Nano-Silicon/Carbon Composite Anode Materials Towards Practical Application for Next Generation Li-Ion Batteries, J. Electrochem. Soc. 2015;162:A2509–28

[9] Mastali M, Farkhondeh M, Farhad S, Fraser RA, Fowler M, Electrochemical Modeling of Commercial LiFePO 4 and Graphite Electrodes: Kinetic and Transport Properties and Their Temperature Dependence , J. Electrochem. Soc. 2016;163:A2803–16

[10] Jiang Y, Niu Z, Offer G, Xuan J, Wang H, Insights into the role of silicon and graphite in the electrochemical performance of silicon/graphite blended electrodes with a multi-material porous electrode model, J. Electrochem. Soc. 2022.169:020568

[11] Mercer MP, Peng C, Soares C, Hoster HE, Kramer D, Voltage hysteresis during lithiation/delithiation of

graphite associated with meta-stable carbon stackings, J. Mater. Chem. A 2021;9:492–504
[12] Sethuraman VA, Srinivasan V, Newman J, Analysis of Electrochemical Lithiation and Delithiation Kinetics in Silicon, J. Electrochem. Soc. 2013;160:A394–403
[13] Torchio M, Magni L, Gopaluni RB, Braatz RD, Raimondo DM, LIONSIMBA: A Matlab Framework Based on a Finite Volume Model Suitable for Li-Ion Battery Design, Simulation, and Control, J. Electrochem. Soc. 2016;163:A1192–1205
[14] Housel LM, Li W, Quilty CD, Vila MN, Wang L, Tang CR, Bock DC, Wu Q, Tong X, Head AR, Takeuchi KJ, Marschilok AC, Takeuchi ES, Insights into Reactivity of Silicon Negative Electrodes: Analysis Using Isothermal Microcalorimetry, ACS Appl. Mater. Interfaces 2019;11:37567–77
[15] Arnot DJ, Effect of Temperature and FEC on Silicon Anode Heat Generation Measured by Isothermal Microcalorimetry, JElS 2021;168:110509
[16] Vadakkepatt A, Bruggeman's Exponents for Effective Thermal Conductivity of Lithium-Ion Battery Electrodes, 2016;
[17] Larkin JM, McGaughey AJH, Thermal conductivity accumulation in amorphous silica and amorphous silicon, Phys. Rev. B - Condens. Matter Mater. Phys. 2014;89:144303
[18] Queen DR, The specific heat of pure and hydrogenated amorphous silicon, UC Berkeley, 2011; Accessed: May 25, 2022. Available: https://escholarship.org/uc/item/58d766kb.
[19] Tritsaris G, Zhao K, Okeke OU, Kaxiras E, Diffusion of lithium in bulk amorphous silicon: a theoretical study, ACS Publ. 2012;116:22212–16
[20] Yao KPC, Okasinski JS, Kalaga K, Almer JD, Abraham DP, Operando Quantification of (De)Lithiation Behavior of Silicon–Graphite Blended Electrodes for Lithium-Ion Batteries, Adv. Energy Mater. 2019;9:1803380